Shrinking of Anionic Polyacrylate Coils induced by Ca^{2+}, Sr^{2+} and Ba^{2+}: A combined Light Scattering and ASAXS Study

Ralf Schweins[§] , Günter Goerigk[&] and Klaus Huber*

Universität Paderborn, Fakultät für Naturwissenschaften,

Department Chemie, Warburger Str.100

D-33098 Paderborn FRG

e-mail: klaus.huber@upb.de

[&] Institut für Festkörperforschung, Forschungszentrum Jülich Postfach 1913, D-52425 Jülich FRG

[§] Institut Laue-Langevin, LSS Group, B.P. 156, 6 rue Jules Horowitz, F-38042 Grenoble cedex 9, France

Abstract. Anionic polyacrylate chains (NaPA) form precipitates if alkaline earth cations are added in stoichiometric amounts. Accordingly, precipitation thresholds were established for three different alkaline earth cations Ca^{2+}, Sr^{2+} and Ba^{2+}. Close to the precipitation threshold, the NaPA chains significantly decrease in size. This shrinking process was followed by means of combined static and dynamic light scattering. Intermediates were generated by varying the ratio MCl_2/[NaPA] with M denoting the respective alkaline earth cation. All experiments were performed at an inert salt level of 0.01 M NaCl. Similar coil – to – sphere transitions could be observed with all three alkaline earth cations Ca^{2+}, Sr^{2+} and Ba^{2+}. Based on these findings, supplementary conventional and anomalous small angle x-ray scattering experiments using selected intermediates close to the precipitation threshold of SrPA were performed. The distribution of Sr-counterions around the polyacrylate chains in aqueous solution provided the desired scattering contrast. Energy dependent scattering experiments enabled successful separation of the pure-resonant terms, which solely stem from the counterions. The Sr^{2+} scattering roughly reflects the monomer distribution of the polyacrylate chains. Different ratios of the concentrations of [$SrCl_2$]/[NaPA] revealed dramatic changes in the scattering curves. The scattering curve at the lowest ratio indicated an almost coil-like behaviour, while at the higher ratios the scattering curves supported the model of highly contracted polymer chains. Most of X-ray scattering experiments on intermediate states revealed compact structural elements which were significantly smaller than the respective overall size of the NaPA particles.

PACS. 61.10.Eq – X-ray scattering (including) small-angle scattering). 82.35.Rs Polyelectrolytes. 78.35.+c - Brillouin and Rayleigh scattering; other light scattering

1 Introduction

Polyelectrolytes are electrically charged, water soluble macromolecules. Due to intramolecular electrostatic interactions, the dissolved chains are highly extended. Addition of an inert salt screens these interactions and modifies the solubility and conformation of the polyelectrolyte chains. If the inert salt level is high enough, the chains can be described by the model of a random walk, also denoted as unperturbed or Θ-dimensions of the chain [1,2]. For sodium polyacrylate (NaPA) in water, this state is achieved by addition of roughly 1.5 moles of alkali halogenides per liter [3-5].

Contrary to this non-specific screening with inert salts, earth alkaline cations strongly interact with the carboxylate functions of the anionic PA-backbone. The largest body of evidence, provided for such specific interactions, also denoted as complex bonding, deals with the interaction between Ca^{2+} and anionic acrylates. This specific bond formation is driven partly by the liberation of water molecules from the hydration shells around the ionic residuals [6,7]. Complex bonding of the Ca^{2+} also neutralizes the NaPA chains [8-12], increases the hydrophobic nature of the backbone and eventually leads to a chain collapse [11-13]. The chain collapse borders precipitation of the resulting CaPA [8-10]. Therefore, investigation of the collapse mechanism is most promising close to the precipitation threshold [11-13].

By means of combined light scattering and small angle neutron scattering (SANS), it was possible to present first evidence for the existence of CaPA intermediates with pearl necklace like structures [14] in solution. Agreement between scattering experiments and model scattering curves was best under the assumption that intermediates comprise a mixture of single spheres and pearl necklace chains with a very low average number of pearls per polyelectrolyte chain [14-16]. The shrinking process ended with the approach of a compact sphere-like shape [13]. Further indication for highly dense domains within polyelectrolyte chains was provided by NMR experiments [17], by ellipsometry [18], by small angle X-ray [19-22] and anomalous small angle X-ray scattering [11,23], by small angle neutron scattering [24-26] and by AFM [20,27]. Part of the results refers to single chain behaviour under dilute solution conditions [11,17,18,21-24,27]. Various SAXS and SANS experiments, for example, predominantly deal with semi-dilute solutions of the polyelectrolyte [19,20,25,26], which makes conclusions on single chain behaviour in dilute solution difficult. In most cases, the impact of specifically interacting cations was investigated [11,17,22,23,25,26]. In other cases,

contraction of the polyelectrolyte was induced by chemical variation of the charge fraction on the polyelectrolyte chains [18-20], by lowering the pH [21], by addition of an organic solvent to aqueous solutions [24] or by addition of an inert salt [27]. Only some of those authors attempted to explicitly discriminate between compact spheres and pearl necklace chains [18,23,24,27], or at least considered their results to be a consequence of pearl necklace chains [17,20,21]. Although, the AFM technique revealed the first direct evidence of pearl necklace chains [27], results measured with dried films cannot be unambiguously transferred to the original solution. The same principle reservation holds for the ellipsometric study [18]. Thus, the body of experimental evidence on pearl necklace chains and conditions under which pearl-necklace chains may exist is still extremely poor.

Pearl necklace structures are introduced as intermediates of collapsing polyelectrolyte chains by theoretical calculations by Kantor and Kadar [28] and Rubinstein et al.[29]. The pearl necklace shape resulted from an analogy between the shrinking polyelectrolyte chain and the Rayleigh instability of charged oil droplets. The collapse could be induced by a subtle interplay of changes of the solvent quality, of the number of charges per chain and of the strength of electrostatic interactions. A crucial part of the process is the condensation of counterions. However, the range of parameters, where pearl necklace like shapes are likely to occur is fairly narrow [15,30,31]. A necessary prerequisite for the generation of pearl necklace like transition states is a hydrophobic backbone and a possibility to tune the charge of the chains [15,30,31] e. g. by addition of specifically interacting counterions.

If specific interactions between anionic polyacrylate in solution and alkaline earth cations or transition metal cations shall be investigated, small angle X-ray scattering (SAXS) is a highly promising method. Complex bonding fixes the counterions at COO^--residuals and decorates the shrinking chain with a component of high electron density. Thus the chains act as a template and may provide access to their shape. Above this, anomalous small angle x-ray scattering (ASAXS) offers additional information if the wavelength of the scattered X-rays is varied [32-38]. This enabled Goerigk et al. [23] and Ballauff et al. [37,38] for the first time to isolate the scattering factor of the counterions condensing on polyelectrolytes. In the present case, variation of the wavelength changes the scattering contrast of the divalent alkaline earth cations as one component of the scattering particle, at a roughly constant scattering contrast of the anionic chain as the other component. However, this requires extension of preceding results [12-14] on heavier alkaline earth cations.

Thus, the phase behaviour and shrinking process established for the precipitation of NaPA with Ca^{2+} ions [12-14] shall be extended to Ba^{2} and Sr^{2+} in the present investigation. Combined static and dynamic light scattering is applied to locate the phase boundary of the respective MPA precipitation and to characterize the global dimensions of the chains while approaching the phase boundary [13]. The use of three different alkaline earth cations allows for a comparison of cations within the homologous series of alkaline earth cations. At the same time the phase behaviour of the cations with the higher order number allows to design SAXS and ASAXS experiments of the PA shrinking. Hence, sets of solutions with Sr^{2+} including two different NaPA samples were selected for further SAXS and ASAXS experiments. Results are expected to yield further insight into the shape of the PA chains collapsing near the phase boundary.

2 Experimental

2.1 Materials

The NaPA samples were purchased from Polysciences, Eppelheim (Germany). Two NaPA samples with different molar mass were used. Light scattering revealed a weight averaged molar mass of M_w = 950 kD (PA1) and 3300 kD (PA2). The polydispersity index is M_w/M_n = 1.2 for both samples, where M_n and M_w is the number averaged and weight averaged molar mass respectively [5]. The inorganic salts, NaCl and $CaCl_2$, $SrCl_2$ and $BaCl_2$ were purchased from Fluka, Buchs (Switzerland) with puriss. p. a. grade.

2.2 Preparation of Solutions for Light Scattering

Preparation of the solutions for light scattering was performed according to two different procedures (**route 1** and **route 2**). The procedure was introduced elsewhere [13] and will be outlined by means of Sr^{2+} .

Route 1. Preparation of NaPA solutions with Sr^{2+} in aqueous NaCl was performed in two steps. In a first step, a solution of NaPA in bidistilled water with 0.01M NaCl at pH 9 (solution I) was prepared together with another solution of 3mM $SrCl_2$ and 4mM NaCl in

bidistilled water at pH 9 (solution II). The pH was set with 0.01M NaOH. It is noteworthy to mention that both solutions had the same number of cationic charges, which was

$$2[Sr^{2+}]+[Na^{+}]=0.01M \quad (1)$$

After 3 days of storage, equal volumes of both solutions were combined. Thus, a stock solution of NaPA in distilled water with 1.5mM $SrCl_2$ and 7mM NaCl with a pH of 9 was obtained (solution III). In an analoguous way, an amount of solution II was combined with an equal amount of bidistilled water with 0.01M NaCl, resulting in an NaPA-free solution of 1.5 mM $SrCl_2$ and 7 mM NaCl at a pH of 9 (solution IV). Solution IV is denoted as solvent and served as the solvent background for all scattering experiments.

The phase boundary for Sr^{2+}-PA precipitation was approached by diluting the stock solution (III) with the solvent (IV). By means of this procedure [13], different ratios of $[Sr^{2+}]$/[NaPA] were obtained at constant concentrations of $[Sr^{2+}]$ and $[Na^{+}]$. As the shape of the polymer chains in solution depends on the extent of complexation, different ratios correspond to different intermediates, bordering the precipitation threshold of SrPA.

Route 2. In a first step, three different solutions were generated. A NaPA solution was prepared with 0.01 M NaCl and a pH of 9 (solution I). A second solution with pure $SrCl_2$ at pH of 9 was set to $[SrCl_2]$ = 0.005 mM, ready to provide the Sr^{2+} ions. A third solution at pH = 9 contained only NaCl at [NaCl] = 0.01 M (solution III). Finally 10 mL of solution I was combined with X ml of solution II in a 20 ml graduated flask. The flask was filled to the mark with (10-X) mL of solution III. The corresponding solvent background was generated in the same way with 10 mL of solution III instead of solution I. The phase boundary was approached by increasing X in the range of 0 mL < X mL < 10 mL.

2.3 Light Scattering

An ALV 5000E Compact Goniometer System with a 100 mW Nd:YAG laser as a light source was used. The scattering intensity was recorded with a photomultiplier in an angular range of 30° to 150° in steps of 10°. Net scattering intensities of polymers were expressed in terms of the Rayleigh ratio ΔR_θ with ΔR_θ referring to the Rayleigh ratio of the standard toluene at 298.15 K, R = $2.737*10^{-5}$ cm^{-1}. Data from static light scattering (SLS) were evaluated to zero scattering angle according to

$$\frac{K \cdot c}{\Delta R_\theta} = \frac{1}{M_w} + \frac{R_g^2}{3M_w} \cdot q^2 \tag{2}$$

with K being the contrast constant, c the polymer concentration in g/mL, M_w the apparent molecular weight and q the momentum transfer

$$q = \frac{4\pi n}{\lambda_0} \sin\left(\frac{\theta}{2}\right) \tag{3}$$

In Eq.(3), n is the refractive index at 532 nm of 0.01M NaCl being 1.336, λ_0 is the laser wavelength in vacuum being 532 nm and θ is the scattering angle.

Correlation functions from dynamic light scattering (DLS) were evaluated by application of the cumulant method [39] with linear and quadratic terms of the correlation time t. The resulting diffusion coefficients D(q) were extrapolated to zero momentum transfer according to

$$D(q) = D_Z (1 + C R_g^2 q^2) \tag{4}$$

Here, C denotes a dimensionless shape sensitive constant and D_Z is the extrapolated diffusion coefficient. The latter can be transformed into a hydrodynamically effective radius R_h by use of the Stokes-Einstein equation

$$R_h = \frac{k_B \cdot T}{6\pi \cdot \eta} \cdot \frac{1}{D_Z} \tag{5}$$

with k_B being the Boltzmann constant, η = 890.37 μPas the solvent viscosity of 0.01M NaCl and T the absolute temperature.

All samples were located close to the phase boundary where the intramolecular shrinking process may increasingly compete with the onset of precipitation. Thus, care had to be taken to identify and discard samples with aggregates. Identification of the onset of aggregation was achieved by using two criterea, evaluated with LS. The first criterion was a significant

increase of the apparent molar mass detected by SLS. The second criterion was based on the CONTIN analysis of the correlation functions from DLS. The CONTIN method [40] allows for distinguishing different diffusive modes, therefore directly indicating aggregation if a mode in addition to the diffusion of the single chains became observable.

2.4 Preparation of Solutions for SAXS and ASAXS Experiments

SAXS and ASAXS experiments were performed with two NaPA samples, PA1 and PA2. A series denoted SAXS-2 with two different ratios $[Sr^{2+}]/[NaPA]$ was prepared for the higher molar mass sample PA2, at $[Sr^{2+}]$=1mM, according to Route 2. Both solutions were fully characterised by LS prior to the SAXS experiment. The solutions were denoted SAXS-2A and SAXS-2B. Sample SAXS-2B was further apart from the phase boundary than SAXS-2A.

Two series with varying ratio $[Sr^{2+}]/[NaPA]$, denoted as SAXS-1 and ASAXS-1, were prepared with sample PA1. Both series were generated according to Route 1 at a level of alkaline earth cations of $[Sr^{2+}]$=1.5mM. Series SAXS-1 was originally investigated at three different energies to additionally account for anomalous scattering. Corresponding ASAXS results have already been published [23] and we only review the total SAXS curves of series SAXS-1. SAXS-1A thereof, was selected on the basis of detailed LS results. This solution was directly transferred from the light scattering cell into the capillary. A second NaPA solution (SAXS-1B) was investigated without being characterized by LS prior to X-ray scattering experiments. The ratio $[Sr^{2+}]/[NaPA]$ of SAXS-1B was smaller than the one of SAXS-1A. Therefore, SAXS-1B was further apart from the phase boundary than SAXS-1A. The parameters of all solutions selected for SAXS experiments are summarized in Table 1.

A second series of the same sample PA1 included four different ratios $[Sr^{2+}]/[NaPA]$. Each solution was investigated at three different energies. It is this series by means of which we are able to present new ASAXS experiments on the system SrPA. The solutions are denoted ASAXS-1X with X = A, B, C and D indicating increasing distances from the phase boundary. Each solution was carefully characterized by means of light scattering prior and after x-ray scattering. Characterisation before and after the ASAXS experiment allows us for the first time to demonstrate long term stability of the four samples under investigation.

2.5 SAXS and ASAXS Measurements

SAXS and ASAXS-experiments were performed in capillaries from Hilgenberg GmbH, Malsfeld (Germany). NaPA solutions and solvent was measured in glass capillaries. The solvent was 0.01n in Cl^- and contained the same amount of Sr^{2+} ions as the respective NaPA solutions. The capillaries were made of borosilicate glass with an inner diameter of 4 mm and a wall thickness of 0.05 mm, specially designed for ASAXS experiments in the energy range of the K-absorption edge of Sr at 16.105 keV. They were filled through the open end and sealed by fixing an appropriate piece of glass with glue on top of the open end. This glass cap was made from an adequately cut Pasteur pipette which was melted off at the conical end. The sealed capillaries were horizontally mounted onto a sample holder which was screwed into the sample area.

All experiments were performed at the JUSIFA beamline[41] at HASYLAB, DESY Hamburg. The energies used for all three series are summarized in Table 2. The lowest energy of each series was significantly below the K-absorption edge of Strontium at 16.1046 keV and was considered to provide the respective conventional scattering curves (SAXS) referring to the total scattering of the SrPA complex. The columns $f'_{eff}(E)$ and $f''_{eff}(E)$ in Table 2 represent the effective anomalous dispersion corrections calculated from the convolution with the energy resolution of the slit system and the monochromator (Si-311) at the JUSIFA experiment. The values at the energy of the Sr-K-edge are significantly changed compared to the theoretical values obtained from the Cromer-Liberman calculations without taking the limited energy resolution of the experiment into account.

The focus of the present work lies on series ASAXS-1 with sample PA1. For ASAXS-1, the energy dependence of the small angle X-ray scattering near the K-absorption edge of Sr was measured in order to isolate the scattering from the Sr-ions. Measurements were made with a two-dimensional detector at three energies. A q-range from about 0.075 to 2.5 nm^{-1} was covered. Table 2 provides the anomalous dispersion corrections for Sr at the energies used here based on the calculations of Cromer and Liberman [42,43]. These were used to permit the separation of the Sr-related pure-resonant scattering described in detail in [23,44]. Constant background effects due to diffuse scattering of the solvent and due to Resonant Raman Scattering occuring near the K-absorption edge at 16.105 keV have been subtracted from the measured intensities before separating the pure-resonant scattering.

The ASAXS data were processed with the software available at the beamline. The program was used to integrate, to correct for transmission and detector sensitivity, to subtract the background and the dark current. All scattering curves have been calibrated into absolute units (i.e. macroscopic scattering cross-sections in units of cross-section per unit volume $cm^2 / cm^3 = cm^{-1}$).

3 Evaluation of ASAXS Measurements

In the case of a dilute solution of polymers the scattering curve of the polymer is given by [45]:

$$I(\vec{q}) = \frac{N}{V} \cdot I_0(\vec{q}) \cdot \psi(\vec{q}) \tag{6}$$

where N/V is the number of dissolved polymers per volume. $\psi(\vec{q})$ is the structure factor, which describes the influence of interparticle correlation and will not be considered further here (ψ=1) due to the dilute solution of the polymers. The second angular dependent term in Eq.(6)

$$I_0(\vec{q}) = |A(\vec{q})|^2 = A(\vec{q}) \cdot A^*(\vec{q}) \tag{7}$$

is the scattering function of a single particle. In Eqs.(6) and (7) q is the absolute value of the momentum transfer $\vec{q}$ (cf. Eq.(3) for light waves). $A(\vec{q})$ is the scattering amplitude of the particle. In the case of negatively charged polyelectrolytes surrounded by positively charged counterions in dilute solution, the scattering amplitude of a single polymer chain writes:

$$A(\vec{q}) = \int \Delta\rho_{poly}(\vec{r}) \cdot \exp(-i\vec{q}\vec{r}) d^3r + \int \Delta\rho_{Ion}(\vec{r}) \cdot \exp(-i\vec{q}\vec{r}) d^3r \tag{8}$$

with

$$\Delta\rho_{Poly}(\vec{r}) = \Delta f_{Poly} \cdot u(\vec{r}) = (f_{Poly} - \rho_m V_{Poly}) \cdot u(\vec{r})$$
$$\Delta\rho_{Ion}(\vec{r}, E) = \Delta f_{Ion}(E) \cdot v(\vec{r}) = ((f_{0,Ion} - \rho_m V_{Ion}) + f'_{Ion}(E) + i f''_{Ion}(E)) \cdot v(\vec{r})$$
(9)

$\Delta\rho_{Poly}, \Delta\rho_{Ion}$ are the excess electron densities of the polyelectrolyte chains and the counterions calculated from the electron density ρ_m of the solvent and the volumes V_{Poly} and V_{Ion} of the chains and the counterions, while $u(\vec{r}), v(\vec{r})$ are the particle densities of the polymer chains and the counterions respectively. The molecular scattering factor (number of electrons) of the chain f_{Poly} is nearly energy independent, whereas the atomic scattering factor of the counterions shows strong variations with the energy in the vicinity of the absorption edge of the counterion which are taken into account by the so-called anomalous dispersion corrections $f'_{Ion}(E), f''_{Ion}(E)$:

$$\begin{aligned} f_{Poly}(E) &\approx \text{const} \\ f_{Ion}(E) &= f_{0,Ion} + f'_{Ion}(E) + i f''_{Ion}(E) \end{aligned} \qquad (10)$$

Calculating the scattering intensity due to Eqs.(7-9) and averaging over all orientations of the polymer yields:

$$\begin{aligned} I_0(q,E) = {} & 4\pi\Delta f_{Poly}^2 \iint_{V_p} u(\vec{r})u(\vec{r}\,')\frac{\sin(q|\vec{r}-\vec{r}\,'|)}{q|\vec{r}-\vec{r}\,'|}d^3r\,d^3r' \\ & + 4\pi \cdot 2\Delta f_{Poly}(f_{0,Ion} - \rho_m V_{Ion} + f'_{Ion}(E)) \iint_{V_p} u(\vec{r})v(\vec{r}\,')\frac{\sin(q|\vec{r}-\vec{r}\,'|)}{q|\vec{r}-\vec{r}\,'|}d^3r\,d^3r' \\ & + 4\pi\Delta f^*_{Ion}(E) \cdot \Delta f_{Ion}(E) \iint_{V_p} v(\vec{r})v(\vec{r}\,')\frac{\sin(q|\vec{r}-\vec{r}\,'|)}{q|\vec{r}-\vec{r}\,'|}d^3r\,d^3r' \end{aligned} \qquad (11)$$

Eq.(11) is composed of three terms: (i) the scattering of the polymer chains; (ii) the cross-term originating from the superposition of the scattering amplitudes of the polymer and the counterions; (iii) the scattering of the counterions, which contains the so-called pure-resonant scattering of the counterions. By measuring the scattering curves at two energies in the vicinity of the absorption edge of the counterions and subtracting the two scattering curves the non-resonant scattering contribution of the polymer is vanishing:

$$\Delta I_0(q,E_1,E_2) = I_0(q,E_1) - I_0(q,E_2)$$
$$= 4\pi \cdot 2\Delta f_{Poly}(f'_{Ion}(E_1) - f'_{Ion}(E_2)) \iint_{V_p} u(\vec{r})v(\vec{r}') \frac{\sin(q|\vec{r}-\vec{r}'|)}{q|\vec{r}-\vec{r}'|} d^3r d^3r' \quad (12)$$
$$+ 4\pi(\Delta f^*_{Ion}(E_1) \cdot \Delta f_{Ion}(E_1) - \Delta f^*_{Ion}(E_2) \cdot \Delta f_{Ion}(E_2)) \iint_{V_p} v(\vec{r})v(\vec{r}') \frac{\sin(q|\vec{r}-\vec{r}'|)}{q|\vec{r}-\vec{r}'|} d^3r d^3r'$$

Now the scattering function is reduced to the resonant contributions - the so-called **separated scattering** - but the scattering of the polymer is still present in the cross-term. To overcome this drawback, a measurement at a third energy can be performed and when subtracting the separated scattering obtained at the two energies E_1, E_3 from the separated scattering obtained at the two energies E_1, E_2 the cross-term is vanishing and only the pure-resonant scattering contribution of the counterions remains:

$$\frac{\Delta I_0(q,E_1,E_2)}{f'_{Ion}(E_1) - f'_{Ion}(E_2)} - \frac{\Delta I_0(q,E_1,E_3)}{f'_{Ion}(E_1) - f'_{Ion}(E_3)}$$
$$= 4\pi[f'_{Ion}(E_2) - f'_{Ion}(E_3) + \frac{f''^2_{Ion}(E_1) - f''^2_{Ion}(E_2)}{f'_{Ion}(E_1) - f'_{Ion}(E_2)} - \frac{f''^2_{Ion}(E_1) - f''^2_{Ion}(E_3)}{f'_{Ion}(E_1) - f'_{Ion}(E_3)}] \iint_{V_p} v(\vec{r})v(\vec{r}') \frac{\sin(q|\vec{r}-\vec{r}'|)}{q|\vec{r}-\vec{r}'|} d^3r d^3r'$$

(13)

Due to Eq.(13) ASAXS is a technique to access directly the scattering of the counterions. From Eq.(13) the structural information of the counterion distribution surrounding the macroions can be obtained.

4 Results and Discussion

4.1 Location of the Phase Boundary by Light Scattering

Fully dissociated sodium salts of polycarboxylates can be precipitated by addition of low amounts of an alkaline earth cation. The amount of alkaline earth cations $[M^{2+}]_c$ required for precipitation follows a linear relationship [9,12] with the polymer concentration expressed in terms of the molar concentration of anionic charges COO^- expressed as $[NaPA]_c$.

$$[M^{2+}]_c = m + r_o[NaPA]_c \quad (14)$$

The intersection m corresponds to a lowest critical concentration threshold $[M^{2+}]_c$ necessary to precipitate the polyelectrolyte at infinite dilution. Beyond the threshold m, a slope r_o points to a stoichiometric amount of M^{2+} per COO^- function, necessary to precipitate polycarboxylate chains. Addition of an inert salt increases the intersection m and gradually decreases [9,13] the slope r_o. The latter effect was compatible with the recent findings [10] that the precipitates included a fraction of monovalent cations in addition to M^{2+}. This fraction obviously increases with increasing [NaCl].

In a first step, a concentration regime close to the precipitation line of M^{2+}-PA has to be identified at a given inert salt level. This concentration regime was expected to provide the most significant conformational changes of the M^{2+}-PA chains. Identification of the appropriate concentration regime was performed by means of combined SLS and DLS. SLS yielded z-averaged radii of gyration R_g characterizing the geometric size of the shrinking coils. Supplementary DLS data led to a distribution of hydrodynamically effective radii and a z-averaged value R_h thereof. With a set of samples at varying $[M^{2+}]$/[NaPA], the point with the minimum value in R_g was located and interpreted as the precipitation threshold. The threshold coordinates ($[M^{2+}]_c$, $[NaPA]_c$) were confirmed by DLS. As soon as aggregation sets in, SLS exhibited an increase of the apparent molar mass and DLS revealed a second particle fraction with an R_h value much larger than the one of the single chains.

For the system under investigation, the inert salt level was set to [NaCl] = 0.01M. In order to evaluate the impact of cation variation within a homologuous series, a comparative investigation was performed with Ca^{2+}, Sr^{2+} and Ba^{2+} added to PA2. All data are established along route 1. Results are summarized in Figure 1 and Table 3. Clearly, the phase boundaries lie on top of each other. A closer look reveals a slight decrease of the slope r_0 of Eq.(1) according to $Ca^{2+} > Sr^{2+} > Ba^{2+}$, which indicates that the larger the divalent earth alkaline cation is, the smaller is the stoichiometric amount of M^{2+} necessary to precipitate NaPA. The trend is opposite to the observations of Pochard et al.[10] who found an increase of the amount of M^{2+} per COO^- groups required to precipitate NaPA if Ba^{2+} ions are used instead of Ca^{2+}.

Once the precipitation line with its adjoining one-phase regime was established, structural changes of dilute PA chains close to the precipitation threshold were characterized in a second step. Combined SLS and DLS, revealed a decrease of the radius of gyration R_g and the hydrodynamically effective radius R_h when the precipitation line is approached. From both radii, two dimensionless parameters can be calculated which are extremely valuable for the investigation of shape transformations along the shrinking process [13].

The first parameter α_s is the ratio of the radius of gyration R_g of any intermediate along the approach to the phase boundary and the radius of gyration $R_g(\Theta)$ under Θ-conditions. The value for $R_g(\Theta)$ was determined experimentally [5] in 1.5 M NaCl.

$$\alpha_s = R_g/R_g(\Theta) \qquad (15)$$

This ratio quantifies the extent of expansion or shrinking of the intermediates in terms of the unperturbed chain. The second parameter ρ compares [46] the radius of gyration R_g of any intermediate along the approach to the phase boundary with the corresponding hydrodynamic radius R_h.

$$\rho = R_g/R_h \qquad (16)$$

The ρ-ratio is expected to be highly sensitive to the shape of the shrinking coil.

In a preceding paper [5], detailed molar mass dependent experiments with NaPA were performed at various inert salt levels. The resulting averages were ρ =1.84 and ρ =1.53 at [NaCl]=0.1M and [NaCl]=1.5M respectively. A similar drop in ρ was observed with neutral polymers when decreasing the solvent quality from good to Θ-conditions [47-49]. The small discrepancies in the absolute values may at least in part be due to the different polydispersities. For the NaPA samples under present investigation, the ratio of the weight averaged and number averaged molar mass is M_w/M_n=1.2 which is larger than the polydispersity of the investigated neutral polymers [47-49].

Specific interactions of M^{2+} ions with the carboxylate functions are expected to cause drastic changes in the conformation of NaPA chains, which have to be distinguished from the regular screening effects imposed by an inert salt [5]. Isolation of these specific interactions could be

achieved by introducing the M^{2+} ions via replacing the corresponding amount of inert Na^{+} ions at constant overall concentration of cationic charges. Thus, regular screening could be kept constant while inserting the specifically interacting M^{2+} ions.

As is outlined in Figure 2, results on the homologuous series of M^{2+} in 0.01 M NaCl confirmed earlier findings [13] on Ca^{2+}. Constant ρ ratios were observed over a regime of shrinking of $1.0 > \alpha_s > 0.4$ for all three cations. Only when the shrinking ratios α_s dropped below 0.4, the sphere limit of 0.77 was approached in a steep descent. In all three data sets of Figure 2 an additional curve is included. This curve corresponds to a plot derived from experimental data of poly-(N-isopropylacryamide) (PNIPAM) in water [50]. At $T = 30.6\ °C$, water is a Θ-solvent for PNIPAM and the resulting curve represents the collapse of a neutral polymer chain if the Θ-point is crossed. The curve begins with $\rho = 1.5$ at $\alpha_s = 1$, gradually decreasing to a value of $\rho = 0.77$ at shrinking ratios close to $\alpha_s = 0.2$, which is compatible with a coil to sphere transition. PNIPAM thus provides an excellent reference system. This indicates a mechanism of NaPA-coil shrinking in 0.01 M NaCl, which deviates from the mechanism for neutral PNIPAM in a Θ-solvent and which is independent of the type of alkaline earth cation in the first place. In principle, ρ values, which are independent of α_s over a large regime of shrinking down to $\alpha_s \sim 0.4$, are compatible with self similar intermediates or increasingly anisotropic intermediates. In the latter case, the impact of shrinking on the value of ρ would be balanced by an increasing anisotropy.[51,52]

Unfortunately, data of the homologous series of M^{2+} under present investigation were of changeable quality. Data from Sr^{2+} ions scattered slightly more than those of Ca^{2+} (Figure 2a and 2b). Barium as the largest cation in the row exhibited a trend (Figure 2c) which was of even better quality than Ca^{2+}. Yet, SAXS experiments were only feasible at the K-edge of Sr^{2+}.

4.2 Total SAXS curves

In order to select appropriate solutions for SAXS experiments, three series of solutions of NaPA with Sr^{2+} were generated along approaches to the corresponding phase boundary. Approaches were performed with two different molecular weights (PA1 and PA2). Solutions where the collapse was not yet completed, i.e. where the limit of a spherical shape was not yet reached, were considered to be highly interesting shapes. Such shapes were signified by a

large degree of shrinking, i. e. by values of α_s significantly smaller than 1.0 but with ρ-values still larger than 1.0. In principle, both parameters were accessible by light scattering.

Figure 3A shows the SAXS curves of series SAXS-2 close to the phase boundary of PA2 with a molar mass of 3300 kD. Both curves almost lie on top of each other. They exhibit a shoulder bordering a steep descent which can be well described by a power law according to Porod [53]. This is a characteristic feature of compact objects with smooth surfaces. Interpretation in terms of spherical particles is at hand. A shallow kink can be discerned at $q_{Min} = 0.3$ nm^{-1}, which may correspond to the first minimum of the particle scattering factor of a sphere [16], blurred by polydispersity effects and irregularities in shape. Using the well known relationship

$$R = 3\pi/2q_{Min}\,, \qquad (17)$$

a sphere radius of R = 15.7 nm can be estimated for both intermediates [16,54]. This value has to be compared with the radii of gyration R_g = 22.2 nm and 31.2 nm and the hydrodynamically effective radii R_h of 18.2 nm and 21.1 nm respectively, which characterize the overall size of the polymer chains. Noticeably, hydrodynamic radii as well as radii of gyration are larger than the estimated sphere radius thus indicating particles with larger overall dimensions than the spherical element revealed by the SAXS curves.

A further series of solutions was selected from sample PA1 with a molar mass of 950 kD denoted SAXS-1. The series SAXS-1 includes total SAXS curves of two concentrations. Sample properties from both selected concentrations are summarized in Table 1. Both SAXS curves were recorded [23] at the energy of 15.507 keV and are shown in Figure 3B. Unlike to sample PA2, comparison of the two curves of sample PA1 indicates striking differences between the corresponding shapes.

In the solution SAXS-1B, the scattering curve follows a power law close to $I_o(q,E_1) \sim q^{-2}$, typical for a structure with a Gaussian density profile. The latter profile has been well established for flexible polymer coils. The solution SAXS-1A shows a much steeper descent. As in the case of series SAXS-2 (sample PA2), a decay close to a q^{-4} power law suggests a structure with a sharp surface. A value of $q_{Min} = 0.25$ nm^{-1} for SAXS-1A (Fig.3b) inserted in Eq.(17) yields a value of R = 19.0 nm. The differences observed for the two solutions SAXS-

1A and 1B are in line with the anticipated shrinking process. In SAXS-1B, the ratio $[Sr^{2+}]/[NaPA]$ is lower than in SAXS-1A which locates SAXS-1A closer to the phase boundary. As expected, the estimated size of 19 nm is in agreement with the pearl size extracted from the resonant part in a preceding work [23].

At this point, we have to stress two drawbacks of the preceding experiments [23]: (i) radii of gyration measured by LS exhibit uncertainties which significantly exceed 10% once they approach values of 20 nm; (ii) characterisation by LS was performed a few days before the ASAXS experiment and slight changes between LS and ASAXS experiments cannot be fully excluded.

In order to consider these drawbacks and to put the findings on a broader base, four additional intermediate states were generated with PA1 in series ASAXS-1 and investigated at three different energies. This time, the selected concentrations were characterised by means of LS prior to and after the SAXS and ASAXS experiments. Crude interpretation of the respective total scattering curves at E = 15507 keV with Eq.(17) and $q_{Min} \approx 0.3 nm^{-1}$ in all four cases led to R close to 16 nm. As with series SAXS-2, the respective size is significantly smaller than the overall size of the polyelectrolyte chains estimated by light scattering (Table 4).

4.3 ASAXS at the phase boundary

In the case of series ASAXS-1, separation of the pure-resonant curves could be successfully carried out. The pure-resonant curves can unambiguously be attributed to the Sr^{2+} counterions. Fig.4 compares the total scattering curves with the corresponding mixed resonant or separated scattering curves (Eq.(12)) and the form factor of the pure-resonant curves (Eq.(13)). Qualitatively spoken, the trends of all three curves are similar confirming our expectation that the Sr counterions densely stick to the polyanionic chains thus reflecting essential features of chain structure.

In order to interpret the pure-resonant curves, model fits were performed with theoretical curves for polydisperse spheres

$$S_{Ion}(q) = const \int_0^\infty P(M) \cdot \left(\frac{4\pi R^3}{3} \frac{3(\sin(qR) - qR\cos(qR))}{(qR)^3}\right)^2 \cdot dR \tag{18}$$

The bracket in the integral contains the form factor of a single sphere of size R.[54] Polydispersity was considered by means of a Schulz-Flory type of distribution P(M) [55]

$$P(M) = \left(\frac{z+1}{M_w}\right)^{z+1} \frac{M^z}{\Gamma(z+1)} \exp\left(-\frac{(z+1)M}{M_w}\right) \tag{19}$$

The particle mass M in Eq.(18) and (19) is proportional to R^3 . Polydispersity is fixed by z = $1/(M_w/M_n-1)$ with M_w and M_n the weight averaged and number averaged particle mass and R_z is the mean radius of the spheres calculated from the z-averaged radius of gyration according to $R_z^2 = R_g^2 \cdot 5/3$. As is demonstrated in Figure 5 for ASAXS-B1 and ASAXSA-C1, the resulting curves satisfactorily describe the experiments. Values for R_z are summarized in Table 4. All R_z values lie close to the results obtained with q_{Min} in Eq.(17) and are significantly smaller than the overall size of the collapsing chains. This clearly supports the fact that the objects indicated by the total scattering curves and by the pure-resonant curves correspond to spherical sub-particles formed within the larger PA chains.

In order to further support this statement, experimental scattering curves shall be described with particle scattering factors which are capable to reproduce the trend of scattering curves and at the same time are consistent with particle size values established by light scattering. The latter condition requires particle sizes which are significantly larger than the size from the fit with model spheres. To this end we used the model of a dumbbell as the shortest representative for pearl necklace chains [16]. The same concept has already been applied to SANS data on the same system [14].

This goal was achieved by using 16 nm for the pearl size in the first place and by applying a distance A = 40 nm between two connected pearls which results in a radius of gyration identical to the one provided by light scattering. Although this procedure has been applied to all four solutions we confined explicit representation to ASAXS-1B and ASAXS-1C because results are essentially the same in all four cases. As is clearly demonstrated by Figure 5b and

6b, the theoretical curve of a monodisperse dumbbell correctly reproduces the section between 0.07 nm^{-1} < q < 0.2 nm^{-1}. At higher q the theoretical curve exhibits sharp minima caused by the regular spherical pearls and smeared in the real system due to shape irregularities and a polydispersity of the sphere size.

Significant improvement is achieved if the dumbbell is mixed with spheres. In the examples of Figure 6, this is performed by mixing a monodisperse dumbbell with a monodisperse sphere. The pearl size in the dumbbell was set to R = 12.7 nm and its distance to the neighbouring pearl to A = 50 nm. The size of the sphere was chosen to be R = 16 nm resulting in the same volume as the dumbbell. Weighting factors of the scattering curves of the dumbbells and spheres was 0.6 and 0.4 respectively. This composition, together with the pearl distance A was selected to yield a radius of gyration in line with the light scattering results from the respective concentrations. Although the theoretical curves deviate slightly more in the intermediate regime of q = 0.2 nm^{-1} a qualitative description of the experiment is now extended to q = 0.5 nm^{-1}, covering a regime of 0.07 nm^{-1} < q < 0.5 nm^{-1}.

In a final attempt, monodisperse dumbbells are mixed with a polydisperse spherical component. Similar mixtures were found already by Limbach and Holm with computer simulations.[15] The z-averaged radius of gyration of the spheres is R_g = 12.4 nm. This R_g value corresponds to an averaged value of the sphere radius of R = 16 nm. The polydispersity is determined by z=5. Pearl size R and pearl distance A in the dumbbell is 16 nm and 55 nm respectively. In calculating the total scattering curve, both component scattering curves are weighted with 0.5. Again weight factors and pearl distance A are selected to reproduce the correct overall size of the particles predetermined by light scattering. In comparison to the binary system with monodiperse components, the theoretical curves based on a polydisperse spherical component improve description in the intermediate regime. Thus, a description of persisting quality is provided, now over the extended regime of 0.07 nm^{-1} < q < 0.2 nm^{-1} (Figure 7).

Real fits with model mixtures have been deliberately avoided in the above described procedure for the following reasons: Aside from pearl size and pearl distance, additional parameters like the composition of multi component structures, size polydispersity and shape irregularities have an influence on the system. The fact, that experimental curves start at a q-value which is too high to include these essential aspects of the overall shape [16] renders

such a fit almost useless. However, SAXS and ASAXS curves provide several interesting features of the collapsing polyacrylate chains: (i) condensation leads to dense structures with spherical (sub-)particles; (ii) SAXS and ASAXS provide an indirect indication of the existence of an elongated second component explaining the large overall particle size. Such a component may be a pearl necklace structure. Possibly the form factor of the pure-resonant scattering, indicates a higher correlated structure, which is suggested when interpreting the correlation maximum at 0.01 $Å^{-1}$ and the shoulders in the q-range between 0.02 and 0.03 $Å^{-1}$ (Fig.4).

5 Summary

The present work extends earlier findings [13] of the phase behaviour of NaPA chains in the presence of various amounts of Ca^{2+} cations and conformational changes of those chains in the proximity of the phase boundary. Extension considers Sr and Ba cations making accessible a comparison of precipitation thresholds in 0.01 M NaCl following Eq(14). Although the phase boundaries lie on top of each other, the amount of M^{2+} required to precipitate the PA chains slightly decrease along $Ca^{2+} > Sr^{2+} > Ba^{2+}$. Light scattering at these phase boundaries lead to normalised plots of the dimensionless size parameters ρ versus α which exhibit the same trend for all three cations. This common trend suggests an anisotropic shape over a large regime of shrinking turning abruptly to a compact sphere at the respective phase boundary. At the same time light scattering enabled selection of intermediates for SAXS and ASAXS experiments.

We succeeded to separate the pure resonant curves for a series of samples with varying ratio $[Sr^{2+}]/[NaPA]$ from energy dependent scattering experiments. Results from this separation fully confirmed the expectation, that the specifically interacting Sr^{2+} counterions adopt a similar spatial distribution as the monomer segments. All but one of the SAXS-curves reflecting total scattering exhibited a steep descent and a shallow kink, located at a momentum transfer denoted as q_{Min}. Under the assumption that this feature can be attributed to compact spherical structures with a finite polydispersity, the following feature appears for most of the solutions under investigation. Size parameters extracted from SAXS and ASAXS are smaller than the overall size of the corresponding polyacrylate chains. A simple

explanation of this difference in size is that SAXS and ASAXS refer to substructures rather than the overall size. As anticipated in theory [15], one way to realize substructures is the (partial) formation of pearl necklace like particles as possible intermediates in the vicinity of the precipitation threshold. These arguments are supported by a successful description of experimental scattering curves by means of model mixtures of spheres and dumbbells. These mixtures reproduce the separated ASAXS curves as good as spheres do but at the same time also result in the correct overall size values of the particles.

Finally, pure resonant scattering ASAXS curves of Sr^{2+} ions could successfully be isolated, in line with an earlier attempt on the same system [23]. These curves indicate a high degree of condensation of the Sr^{2+} ions on length scales related to PA chains which are also present in the same solution. The curves clearly demonstrate that ASAXS can be used to reflect the essential features of a collapsing PA chain if decoration with Sr^{2+} ions can be achieved.

Financial support of the Deutsche Forschungsgemeinschaft, Schwerpunktprogramm "Polyelektrolyte mit definierter Molekülarchitektur" SPP 1009, is gratefully acknowledged.

References

1. Flory, P. J. ; Osterheld, J. E. *J. Phys. Chem.* **1954**, *58*, 653

2. Flory, P. *Principles of Polymer Chemistry*; Cornell University Press: Ithaca, 1953

3. Takahashi, A. ; Yamori, S. Kagawa, I. *Kogyo Kagaku Zasshi* **1962**, *83*, 11

4. Takahashi, A. ; Nagasawa, M. *J. Am. Chem. Soc.* **1964**, *86*, 543

5. Schweins, R. ; Hollmann, J. ; Huber, K. *Polymer* **2003**, *44*, 7131

6. Sinn, C. G. ; Dimova, R. ; Antonietti, M. Macromoelcules **2004**, *37*, 3444

7. Molnar, F. ; Rieger, J. Langmuir **2005**, *21*, 786

8. Ikegami, A. ; Imai, N *J. Polym. Sci.* **1962**, *56*, 133

9. Michaeli, I. J. *Polym. Sci.* **1960**, *48*, 291

10. Pochard, I. ; Foissy, A. ; Couchot, P. *Colloid. Polym. Sci.* **1999**, *277*, 818

11. Sabbagh, I. ; Delsanti, M. ; Lesieur, P. *Eur. Phys. J B* **1999**, *12*, 253

12. Huber, K. *J. Phys. Chem.* **1993**, *97*, 9825

13. Schweins, R. ; Huber, K. *Eur. Phys. J E* **2001**, *5*, 117

14. Schweins, R. ; Lindner, P. ; Huber, K. *Macromolecules* **2003**, *36*, 9564

15. Limbach, H. J. ; Holm, Ch. *J. Phys. Chem. B* **2003**, *107*, 8041

16. Schweins, R. ; Huber, K. *Macromol. Symp.* **2004**, *211*, 25

17. Li, M-J.; Green, M. M.; Morawetz, H. *Macromolecules* **2002**, *35*, 4216

18. Baigl, D. ; Sferrazza, M. ; Williams, C. E. *Europhys. Let*. **2003**, *62*, 110

19. Essafi, W.; Lafuma, F.; Williams, C. E. *J. Phys. II France* **1995**, *5*, 1269

20. Baigl, D. ; Ober, D. ; Qu, A. ; Fery, A. ; Williams, C. E. *Europhys. Let.* **2003**, *62*, 588

21. Heitz, C.; Rawiso, M.; Francois, J. *Polymer* **1999**, *40*, 1637

22. Heitz, C.; Francois, J. *Polymer*, **1999**, *40*, 3331

23. Goerigk, G. ; Schweins, R. , Huber, K.; Ballauf, M. *Europhys. Lett.* **2004**, *66*, 331

24. Aseyev, V. O.; Klenin, S. I.; Tenhu, H.; Grillo, I.; Geissler, E. *Macromolecules* **2001**, *34*, 3706

25. Dubois, E. ; Boué, F. *Macromolecules* **2001**, *34*, 3684

26. Combet, J. ; Isel, F. ; Rawiso, F. *Macromolecules* **2005**, *38*, 7456

27. Minko, S. ; Kiriy, A. ; Gorodyska, G. ; Stamm, M. *J. Am. Chem. Soc.* **2002**, *124*, 10192

28. Kantor, Y.; Kardar, M. *Europhys. Lett.* **1994**, *27* 643

29. Dobrynin, A. V.; Rubinstein, M.; Obukhov, S. P. *Macromolecules* **1996** *29* 2974

30. Schiessel, H. *Macromolecules* **1999**, *32* 5673

31. Uyaver, S. ; Seidel, Ch. *J. Phys. Chem. B* **2004**, *198*, 18804

32. Stuhrmann, H. B. *Advances in Polymer Science* **1985**, 67, 123

33. de Robilliard, Q. ; Guo, X. ; Dingenouts, N. ; Ballauff, M. ; Goerigk, G. ; *Macromol. Symp.* **2001**, *164*, 81

34. Guilleaume, B. ; Ballauff, M. ; Goerigk, G. ; Wittemann, M. ; Rehahn, M. *Colloid Polym. Sci.* **2001**, *279*, 829,

35. Guilleaume, B. ; Blaul, J. ; Ballauff, M. ; Wittemann, M. ; Rehahn, M. ; Goerigk, G. ; *Eur.Phys.J.* **2002**, *E8*, 299

36. Patel, M. ; Rosenfeldt, S. ; Ballauff, M. ; Dingenouts, N. ; Pontoni, D. ; Narayanan, T. ; *PCCP* **2004**, *6*, 2962

37. Dingenouts, N. ; Patel, M. ; Rosenfeldt, S. ; Pontoni, D. ; Ballauff, M. ; Narayanan, T. *Macromolecules* **2004**, *37*, 8152

38. Bolze, J. ; Ballauff, M. ; Rische, T. ; Rudhardt, D. ; Meixner, J. ; *Macromol. Chem. Phys.* **2004**, *205*, 165

39. Koppel, D. E. *J. Phys. Chem.* **1972**, *57*, 4814

40. Provencher, S. W. *Comp. Phys.* **1982**, *27*, 213; *Comp. Phys.* **1982**, *27*, 229

41. Haubold, H.-G. ; Gruenhagen, K. ; Wagener, M. ; Jungbluth, H. ; Heer, H. ; Pfeil, A. ; Rongen, H. ; Brandenburg, G. ; Moeller, R. ; Matzerath, J. ; Hiller, P. ; Halling, H. *Rev.Sci.Instrum.* **1989**, *60*, 1943

42. Cromer, D.T. ; Liberman, D. *J. Chem. Phys.* **1970**, *53*, 1891

43. Cromer, D.T. ; Liberman, D. *Acta Cryst.* **1981**, *A37*, 267

44. Goerigk, G., Williamson, D. L. *J.Appl.Phys.* **2006**, *99*, 084309

45. Glatter, O. ; Kratky, O. Eds. *Small Angle X-ray Scattering* Academic Press, London **1982**

46. Burchard, W. *Advances in Polymer Science* **1983**, *48*, 1

47. Vrentas, J. S. ; Liu, H. T. ; Duda, J. C. *J. Polym. Sci., Polym. Phys. Ed.* **1980**, *18*, 633

48. Schmidt, M. ; Burchard, W. *Macromolecules* **1981**, *14*, 210

49. Huber, K. ; Burchard, W. ; Akcasu, A. Z. *Macromolecules* **1985**, *18*, 2743

50. Wu, C. ; Zhou, S. *Macromolecules* **1995**, *28*, 5388 and 8381

51. Burchard, W. ; Schmidt, M. ; Stockmayer, W. H. *Macromolecules* **1980**, *13*, 580 and 1265

52. Burchard, W. ; Frank, M. ; Michel, E. *Ber. Bunsenges. Phys. Chem.* **1996**, *100*, 807

53. Porod, G. *Kolloid Zeitschrift* **1951**, *124*, 83

54. Rayleigh, Lord *Proc. Roy. Soc.* **1914**, *A 90*, 219

55. Zimm, B. *J. Chem. Phys.* **1978**, *16*, 1099

Figure Captions

Figure 1. Phase boundaries for three different earth alkaline cations in 0.01M [NaCl] : Ca^{2+} (■) ; Sr^{2+} (△) ; Ba^{2+} (●). The polymer is PA2. For better clarity, the phase boundary of Sr^{2+} is shown by itself in the inlet.

Figure 2. ρ-ratios versus extent of shrinking α_s for three different earth alkaline cations : Ca^{2+} **(a)** ; Sr^{2+} **(b)** and Ba^{2+} **(c)**. Different approaches to the phase boundary are denoted in **Fig a**: $[Ca^{2+}]$ = 0.6 $mmolL^{-1}$ (▲); $[Ca^{2+}]$ = 0.8 $mmolL^{-1}$ (▼); $[Ca^{2+}]$ = 1 $mmolL^{-1}$ (◆); $[Ca^{2+}]$ = 0.7 $mmolL^{-1}$ (◀); [NaPA] = 0.803 $mmolL^{-1}$ (●); **Fig. b**: [NaPA] = 0.957 $mmolL^{-1}$ (■); [NaPA] = 0.559 $mmolL^{-1}$ (●); $[Sr^{2+}]$ = 1.0 $mmolL^{-1}$ (▼); [NaPA] = 0.9 $mmolL^{-1}$ (▲); [NaPA] = 1.5 $mmolL^{-1}$of PA1 (◆); **Fig. c**: [NaPA] = 0.55 $mmolL^{-1}$ (▲); [NaPA] = 1.13 $mmolL^{-1}$ (■); [NaPA] = 1.76 $mmolL^{-1}$ (●); $[Ba^{2+}]$ = 0.95 $mmolL^{-1}$ (▼). The curve represents literature data for a coil-globule-transition of neutral polymers below Θ-temperature[36]. Specification of $[M^{2+}]$ or [NaPA] corresponds to route 1 or to route 2 respectively[11]. Unless otherwise stated, PA2 was used as NaPA sample.

Figure 3. Differential X-ray scattering cross sections for series SAXS-1 (A) and SAXS-2 (B). All scattering curves stem from energies far apart from the absorption edge of Sr^{2+} corresponding to total scattering curves of the SrPA adducts. The symbols denote: SAXS-1A with $[Sr^{2+}]/[NaPA]$ = 0.46 (■) ; SAXS-1B with $[Sr^{2+}]/[NaPA]$ = 0.42 (Δ) ; SAXS-2A with $[Sr^{2+}]/[NaPA]$ = 0.667 (■) ; SAXS-2B with $[Sr^{2+}]/[NaPA]$ = 0.651 (Δ). Vertical arrows indicate estimates for q_{Min} used to calculate R according to Eq.(17).

Figure 4. SAXS and ASAXS measurements of the series ASAXS-1 on sample PA1 with $[Sr^{2+}]$=1.5mM at variable ratio $[Sr^{2+}]/[NaPA]$. (A) $[Sr^{2+}]/[NaPA]$ = 0.464; (B) $[Sr^{2+}]/[NaPA]$ = 0.458; (C) $[Sr^{2+}]/[NaPA]$ = 0.4575; (D) $[Sr^{2+}]/[NaPA]$ = 0.451. The symbols denote : (□) total scattering from the polymer and the Sr^{2+} ions at E = 15.507 keV; (Δ) mixed resonant curve according to Eq.(12); (o) formfactor of the Sr^{2+} ions according to Eq.(13). The solid line indicates a q^{-4} power law typical for compact solid particles with smooth surfaces.

Figure 5. Formfactor of the Sr^{2+} ions according to Eq.(13) corresponding to the pure resonant curve for sample ASAXS-B1 (a) and ASAXS-C1 (b). The theoretical curve is a model fit with a polydisperse sphere based on Eq.(18) and (19) with z=5 and R = 15 nm (a) and R = 15 nm (b).

Figure 6. Formfactor of the Sr^{2+} ions according to Eq.(13) corresponding to the pure resonant curve for sample ASAXS-B1 (a) and ASAXS-C1 (b). The two theoretical curves are model curves of a dumbbell with pearl size R=16nm and a pearl-to-pearl distance of A=40nm leading to an overall size of Rg = 23.6nm (—) and of a mixture of monodisperse spheres (weighting factor 0.4) with monodisperse dumbbells with a pearl size R=12.7nm and a pearl-to-pearl distance of A=50nm leading to an overall size of Rg = 22.1nm (---).

Figure 7. Formfactor of the Sr^{2+} ions according to Eq.(13) corresponding to the pure resonant curve for sample ASAXS-B1 (a) and ASAXS-C1 (b). The theoretical curve is a model curve

of a polydisperse sphere based on Eq.(18) and (19) with z=5, Rg = 12.4 nm and R = 16nm (weighting factor 0.5) mixed with a monodisperse dumbbell (weighting factor 0.5) with a pearl size R=16nm and a pearl-to-pearl distance of A=55nm leading to an averaged particle size of R_g = 23 nm.

Tables

Table 1: Specifications of the NaPA solutions used for SAXS experiments. The molar mass of SAXS-1A and 1B is 950 kD (PA1) and of SAXS-2A and 2B 3300 kD (PA2) respectively.

solution	R_g / nm	R_h / nm	q_{Min} /nm^{-1}	ρ	α_s	$\alpha^{1)}$ (DLS)	[NaPA] / mM	$[Sr^{2+}]$/[NaPA]
SAXS-1A	15.9	15.0	0.25	1.06	0.32	0.52	3.25	0.46
SAXS-1B	-	-	-	-	-	-	3.61	0.42
SAXS-2A	22.2	18.2	0.3	1.22	0.275	0.33	1.4997	0.667
SAXS-2B	31.2	21.1	0.3	1.48	0.387	0.38	1.5346	0.651

[1)]Calculated with the corresponding hydrodynamic radii from DLS.

Table 2: Energies and anomalous contributions to the scattering factor f_{Ion} for the three series of $[Sr^{2+}]$/[NaPA] investigated by SAXS and ASAXS. The f'_{Ion}, f''_{Ion} are the theoretical values obtained from the Cromer-Liberman calculations [42,43] without taking the limited energy resolution of the experiment into account. The f'_{eff}, f''_{eff} represent the effective anomalous dispersions corrections estimated form the convolution with the energy resolution of the slit system and the monochromator at the JUSIFA experiment [41].

Series	E / keV	$\Delta E^{1)}$/ eV	f'_{Ion}	f'_{eff}	f''_{Ion}	f''_{eff}
SAXS-1	15.506	599	-2.75	-2.75	0.56	0.56
ASAXS-1	15.507	598	-2.75	-2.75	0.56	0.56
	16.093	12	-6.66	-6.66	0.53	0.53
	16.105	0	-11.66	-10.3	3.77	2.08
SAXS-2	15.512	593	-2.90	-2.90	0.56	0.56

[1)]Difference of the energy of the incident beam and the absorption edge.

Table 3: Parameters of Eq.(1) for phase boundaries of the system PA2 with M^{2+} denoting earth alkaline cations at T = 25°C.

[NaCl]	M^{2+}	m [mmol·L^{-1}]	r_o
0.01	Ca^{2+}	0.549	0.345
0.01	Sr^{2+}	0.563	0.249
0.01	Ba^{2+}	0.622	0.160

Table 4: Size parameters of series ASAXS-1. Radii of gyration R_g and hydrodynamic radii stem from lights scattering experiments prior to (1) and after (2) ASAXS experiments. The radius R_z corresponds to the averaged outer sphere radius extracted from curve fitting with Eq(18). All radii are given in nm. All experiments were performed at $[Sr^{2+}]$ = 1.5mM

solution	$[Sr^{2+}]$/[NaPA]	$R_g(1)$	$R_h(1)$	$R_g(2)$	q_{Min} / nm^{-1}	R_z
ASAXS-1A	0.464	17.3	19.3	24.4	0.38	16
ASAXS-1B	0.458	23.2	23.2	23.0	0.33	15
ASAXS-1C	0.4575	21.3	21	24.0	0.32	15
ASAXS-1D	0.451	30.7	25.2	30.7	0.33	15

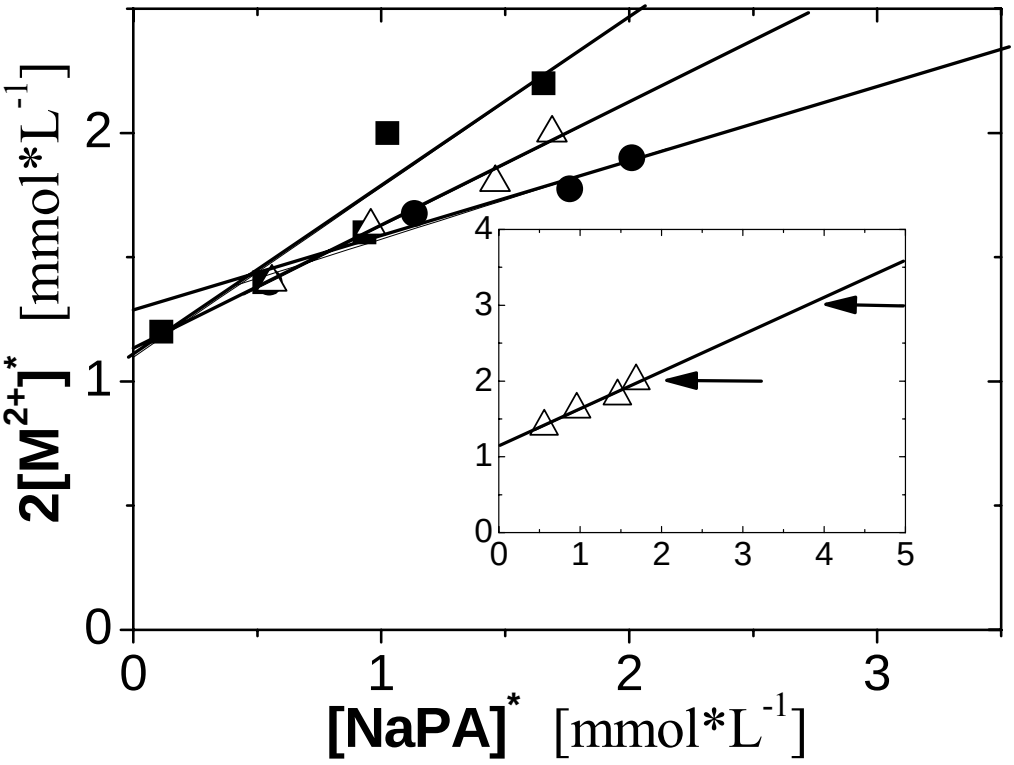

Figure 1

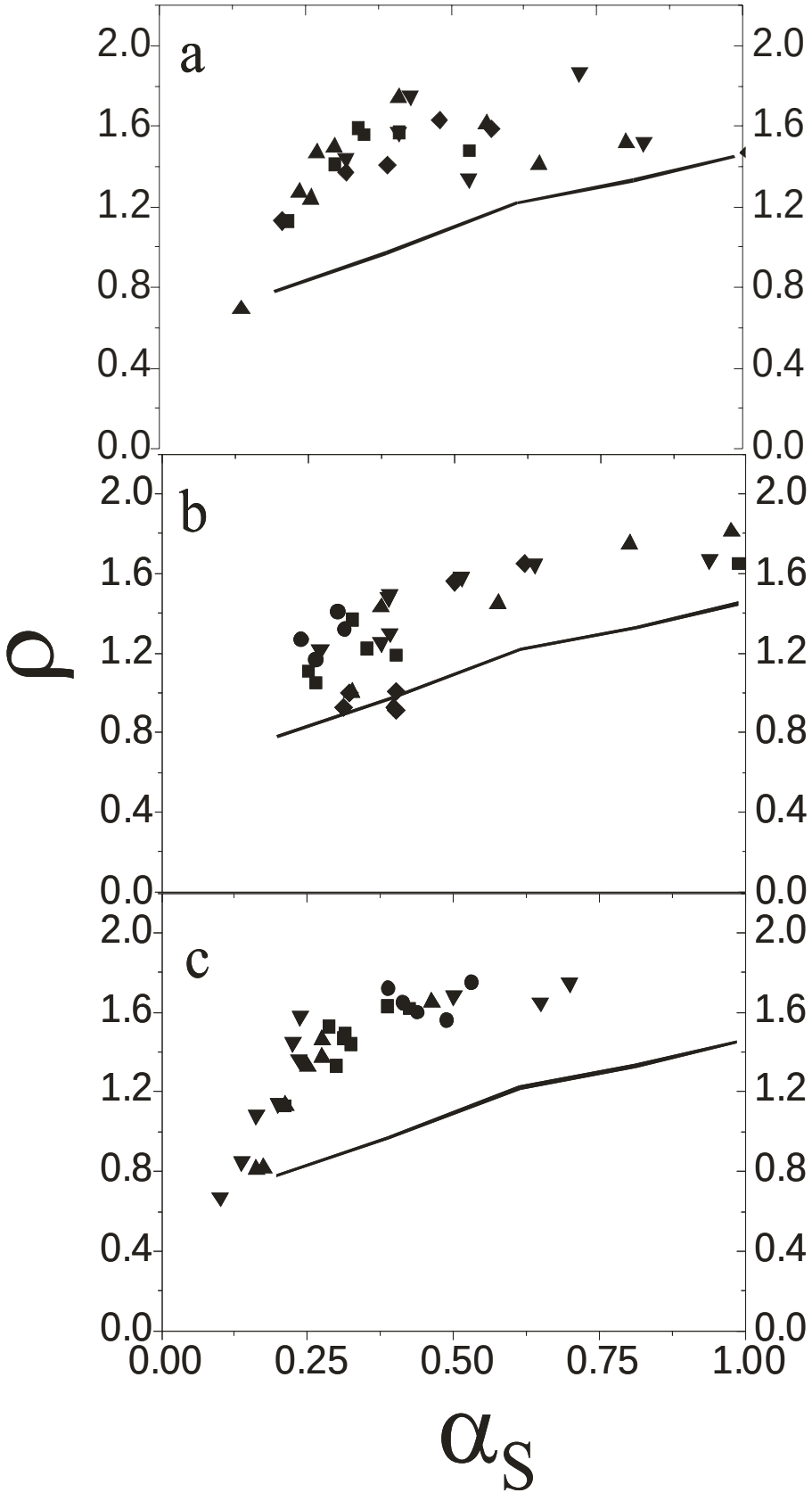

Figure 2

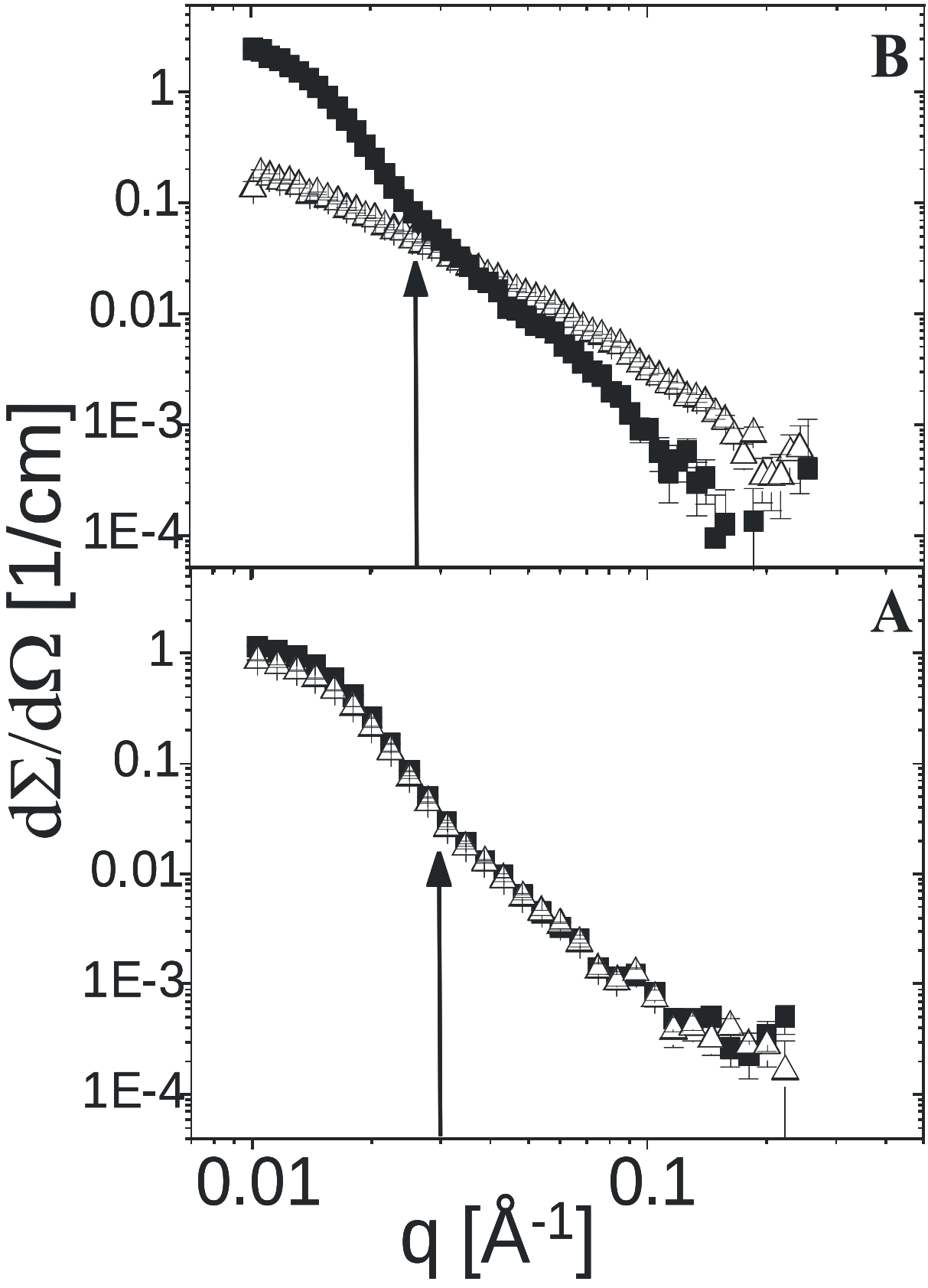
B
A
1
0.1
0.01
1E-3
1E-4
dΣ/dΩ [1/cm]
0.01
0.1
q [Å-1]

Figure 3

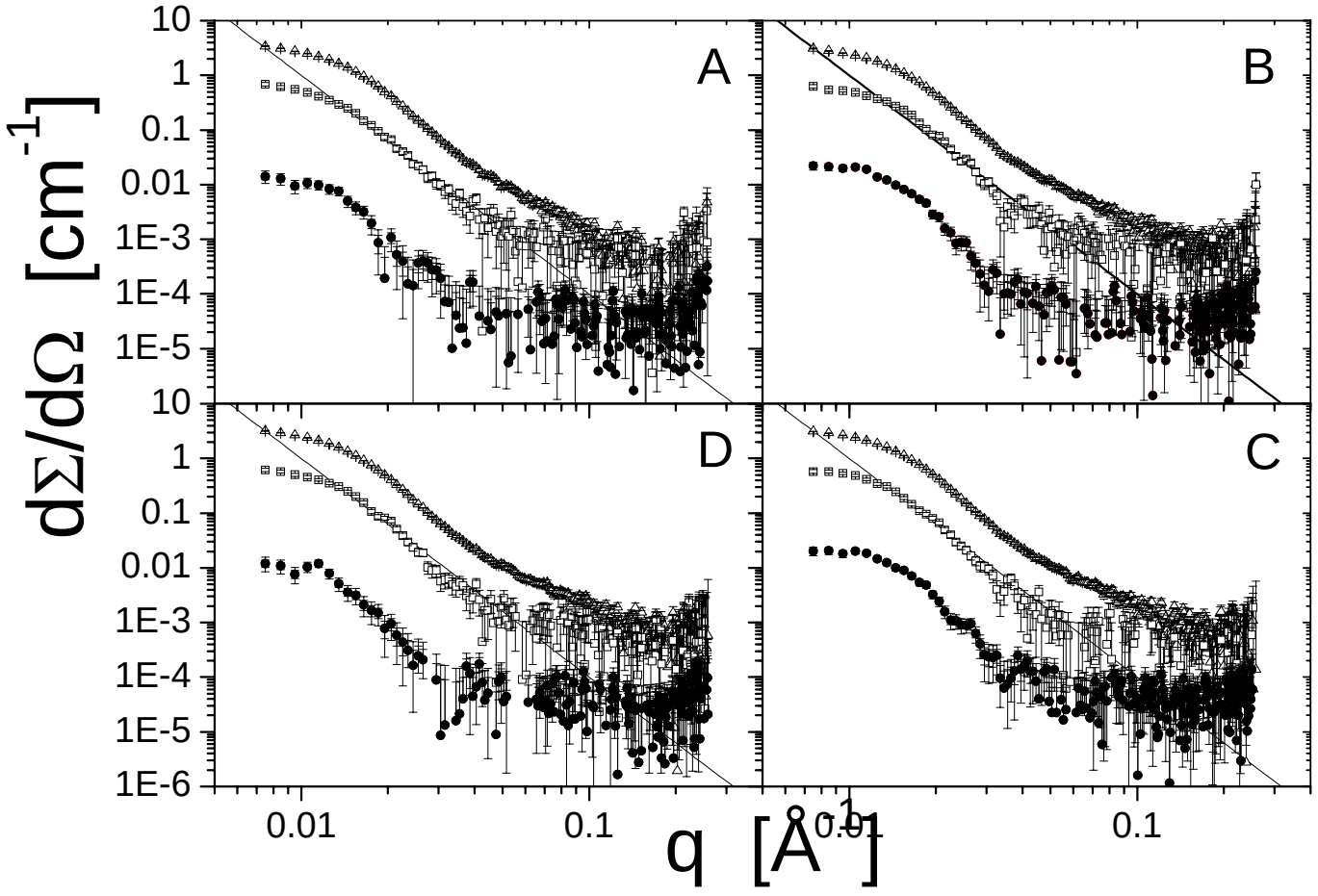

Figure 4

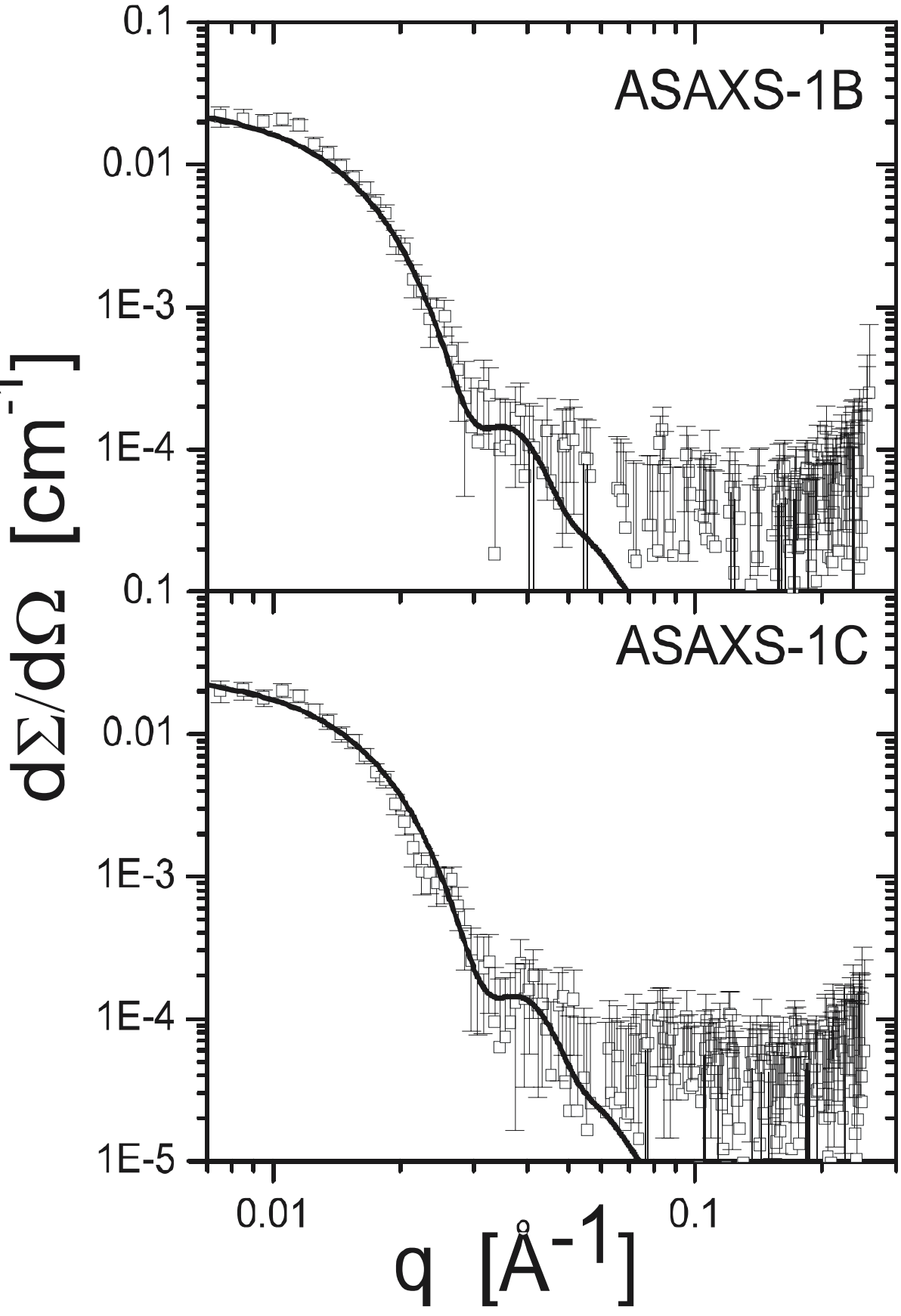
ASAXS-1B
ASAXS-1C
0.1
0.01
1E-3
1E-4
1E-5
dΣ/dΩ [cm-1]
q [Å-1]

Figure 5

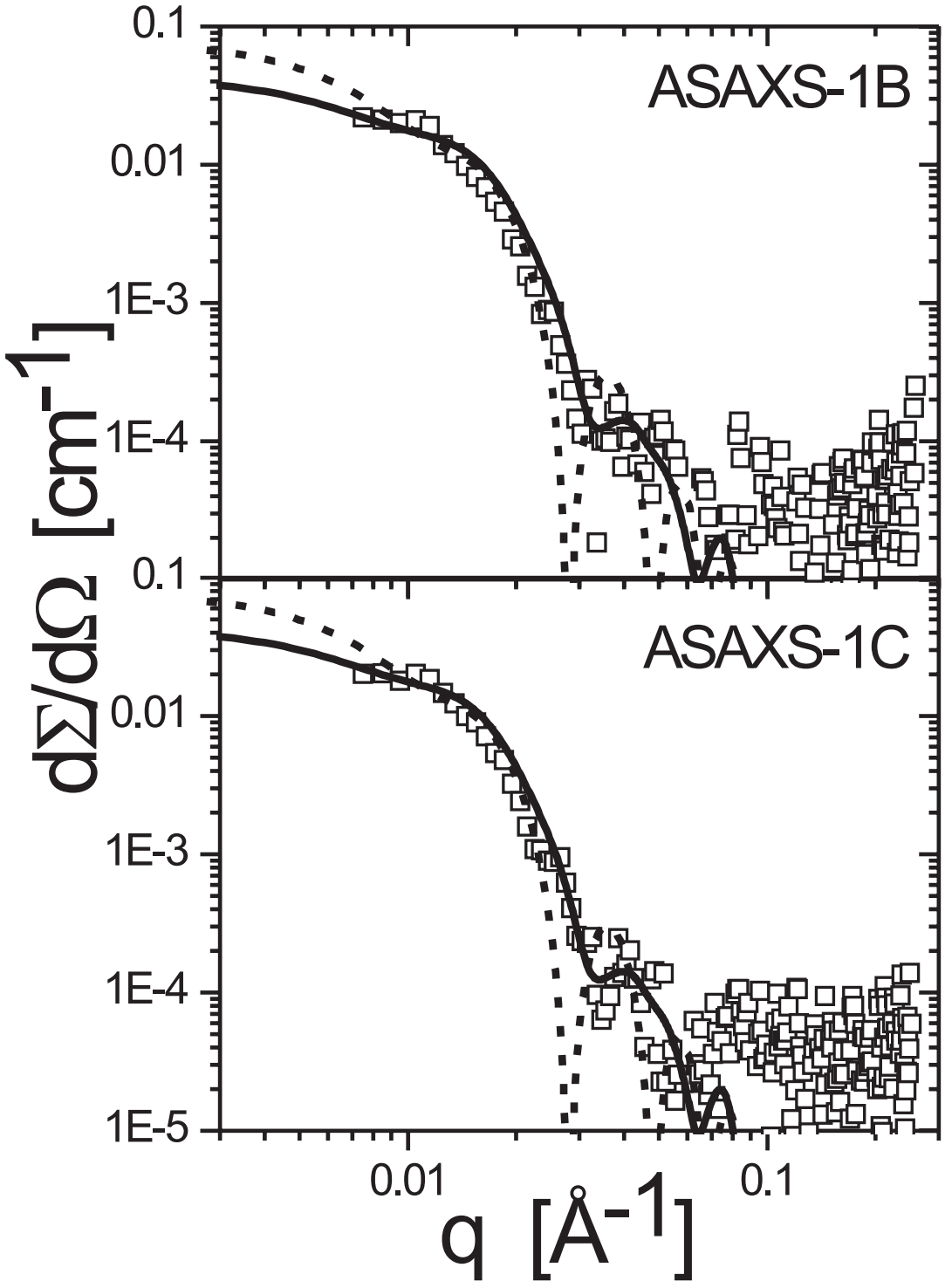

Figure 6

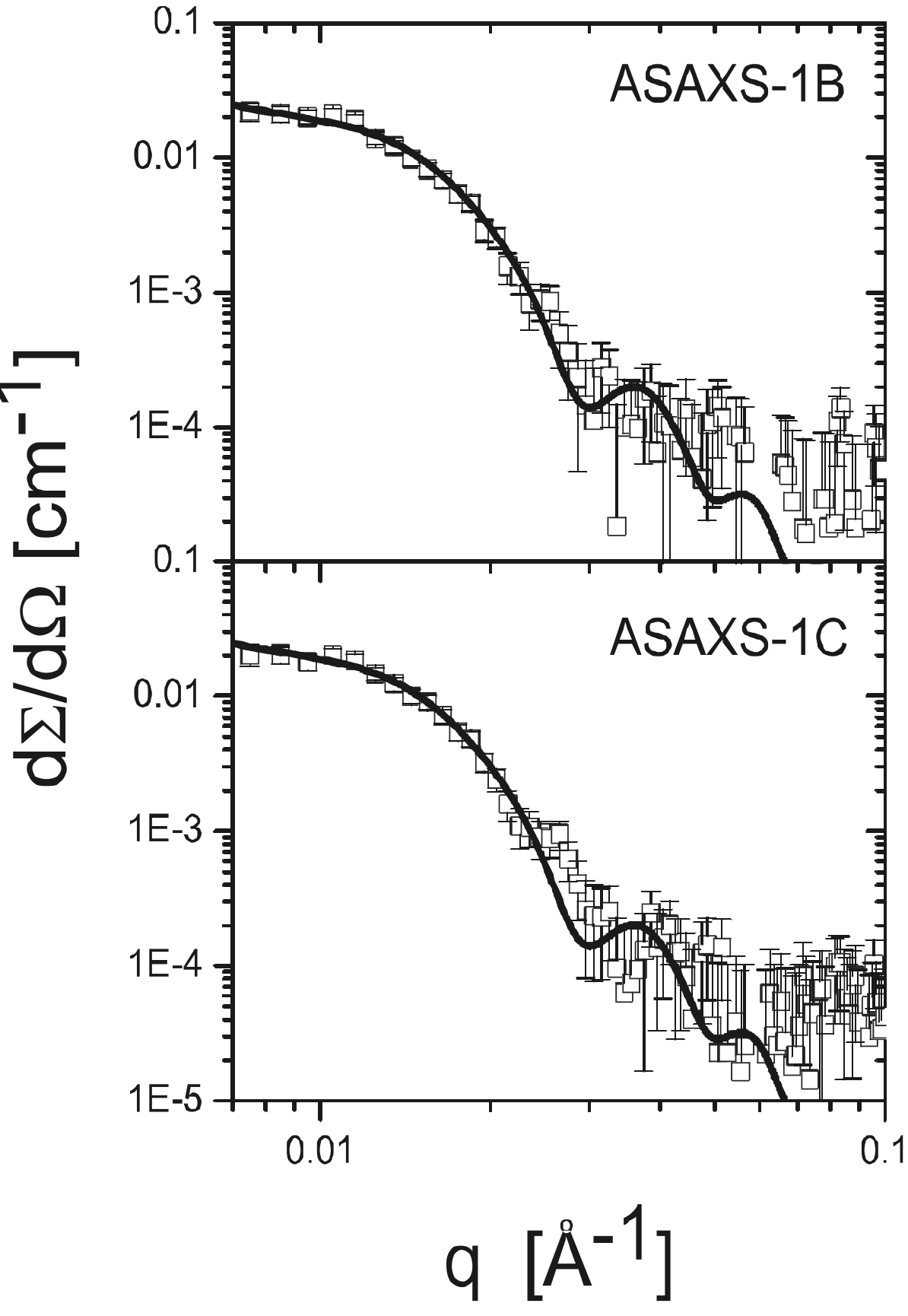

Figure 7